Voltage-induced dynamical quantum phase transitions in exciton condensates

Moon Jip Park[*]

Department of Physics, University of Illinois at Urbana-Champaign, Urbana, Illinois 61801, USA

E. M. Hankiewicz

Institut für Theoretische Physik und Astrophysik, Universität Würzburg, Am Hubland, 97074 Würzburg, Germany

Matthew J. Gilbert

Department of Electrical and Computer Engineering, University of Illinois at Urbana-Champaign, Urbana, Illinois 61801, USA

We explore nonanalytic quantum phase dynamics of dipolar exciton condensates formed in a system of two-dimensional quantum layers subjected to voltage quenches. We map the exciton condensate physics on to the pseudospin ferromagnet model, showing an additional oscillatory metastable phase beyond the well-known ferromagnetic phase by utilizing a time-dependent, nonperturbative theoretical model. We explain the coherent phase of the exciton condensate in quantum Hall bilayers, observed for currents equal to and slightly larger than the critical current, as a stable time-dependent phase characterized by persistent flow of charged order parameter defect in each of the individual layers with a characteristic ac Josephson frequency. As the magnitude of the voltage quench is further increased, we find that the time-dependent current oscillations associated with the charged order parameter defect flow decay, resulting in a transient pseudospin paramagnet phase characterized by partially coherent charge transfer between layers, before the state relaxes to incoherent charge transfer between the layers.

I. INTRODUCTION

The dipolar exciton condensate (DEC) has provided dramatic observations of collective phenomena in a broad swath of host systems, including cold atoms [1–4], semiconductor microcavities [5–7], and semiconductor quantum wells [8–14]. In each of these settings, the Coulomb interaction between spatially segregated charge carriers drives many-body phase transition from the normal Fermi liquid phase to that of a superfluid. Beyond the interesting correlated physics these systems demonstrate, they continue to harbor tantalizing prospects for ultraefficient, electrically tunable information processing systems based on predictions of elevated Kosterlitz-Thouless transition temperatures T_c without the need for external magnetic fields to quench the kinetic energy [15]. These prospects may be directly traced to the realization of new Dirac material systems such as graphene [16–18] and time-reversal-invariant topological insulators [19–23]. In particular, recent experimental work in monolayers of graphene separated by hexagonal boron nitride shows signatures of correlated behavior well above cryogenic temperatures [24].

Of the signatures indicative of the collective phenomena associated with the pseudospin ferromagnetism model (PFM), some of the most dramatic are those found in carrier transport. Within the context of carrier transport, one of the most fundamental parameters is the critical current I_c, the maximum current that the DEC can sustain by simply reorganizing its order parameter. The behavior of the PFM is well understood below I_c, where the system exhibits coherent superfluid flow,

characterized by time-independent coherent current flow and perfect Coulomb drag [25,26]. However, in the region past the critical current, there is a clear deficiency concerning PFM system behavior as voltage quenches resulting in current flow greater than I_c are applied. Naturally, in this regime, the linear response approach is not applicable, and nonperturbative approaches are required. As a corollary, a recent study on dynamical phase transitions in the transverse field Ising model has shown nonanalytic behavior when considering real-time quenches from a ferromagnet to a paramagnet [27] whose behavior is not captured within framework of linear response theory.

Here, we theoretically explore the behavior of a generic PFM system beyond linear response theory. We consider spatially segregated two-dimensional (2D) semiconducting layers using a time-dependent Kadanoff-Baym (TDKB) formalism [28,29] subjected to time-dependent voltage quenches. We are motivated by recent experiments on DEC [8,9], in which, surprisingly, at an interlayer voltage equal to the critical voltage V_c, the condensate behaves in a manner consistent with the fully coherent regime. We explain this observation as a voltage-driven competition between the PFM and a pseudospin paramagnetic (PPM) phase characterized by a time-dependent coherent exciton state which recovers its coherence by periodically launching order parameter defects (OPDs). We define OPDs to be zeros in the excitonic order parameter that contain π discontinuity of the order parameter phase. This regime could serve as an ideal setting for a direct measurement, which should be more definitive than observations of nonzero longitudinal resistance of condensates at finite temperatures [10,11] or indirect influence of topological excitations on Shapiro steps [30]. As the magnitude of the voltage quenches is increased well beyond V_c, we find that the system can no longer relax the superfluid flow by inducing OPDs, the interlayer

---

[*]Also at Micro and Nanotechnology Laboratory, University of Illinois at Urbana-Champaign, Urbana, Illinois 61801, USA.

coherence, which characterizes the PFM phase, is lost, and the layers behave independently, as expected from experiments [8,9]. Moreover, our analysis shows that the condensate in the crossover regime not only will respond to microwave frequencies [30] but shows possibilities as a voltage-tunable electrical oscillator.

This paper is organized in the following manner. We begin in Sec. II with an explanation of the methods and approximations that we have utilized to explore the nonequilibrium time-dependent dynamics of the DEC as a function of bias. In this paper, we endeavor to understand the physics of the DEC within spatially segregated systems through the use of the PFM [31]. Using the pseudospin language, the layer degree of freedom, either top or bottom, is mapped onto an $s = 1/2$ spin in which the top-layer quasiparticles have pseudospin up ($|\uparrow\rangle$) and bottom-layer quasiparticles have pseudospin down ($|\downarrow\rangle$). In Sec. III, we present the numerical results of our self-consistent time-dependent quantum transport calculations of two coupled 2D layers, which are the main subject of this paper. We show that our time-dependent method qualitatively reproduces the well-known interlayer transport characteristics of exciton condensates in the quantum Hall regime as the system transitions from the coherent PFM phase to the incoherent PPM phase [8]. Furthermore, we show the existence of an additional oscillatory metastable phase that exists beyond an interlayer voltage that is beyond the PFM phase and prior to the onset of the PPM phase resulting from interlayer-exchange-related destabilization of the steady-state transport. We attribute the existence of this metastable state to a persistent flow of charged OPDs in each layer with a characteristic ac Josephson frequency. In Sec. IV, we summarize our results and conclude.

II. METHODOLOGY

A. System and Hamiltonian

We begin in Fig. 1(a), where we schematically picture the system of interest. We consider a system consisting of two 2D semiconducting layers in which the top layer is assumed to contain electrons and the bottom layer is assumed to contain an equal population of holes. For simplicity, we assume that the layers are free from disorder, and the system temperature for all of our simulations is set to the zero-temperature limit or, $T_{sys} = 0$ K. We attach contacts to the left and right ends of the top layer (C_{TL} and C_{TR}) and the bottom layer (C_{BL} and C_{BR}) from which we inject and extract currents. The contacts are modeled as semi-infinite layers with the same Hamiltonian parameters as the device region described below. Within our system, we apply bias to the top left contact V_{TL} and set all of the other contact potentials to be zero, or $V_{TR} = V_{BL} = V_{BR} = 0$. In this bias configuration, all carriers are injected from C_{TL} when $V_{TL} < 0$, while the injected carriers are then extracted via the other three contacts. Similarly, all carriers are extracted from the coupled wire system through C_{TL} when $V_{TL} > 0$. With the system defined, we may now write the tight-binding Hamiltonian for a single layer using a simple 2D single subband chain as

$$H_{T,B} = \sum_{i,j} -(\tau c_{i,j}^\dagger c_{i,j\pm 1} + \tau_{\mathrm{trans}} c_{i,j}^\dagger c_{i\pm 1,j}), \quad (1)$$
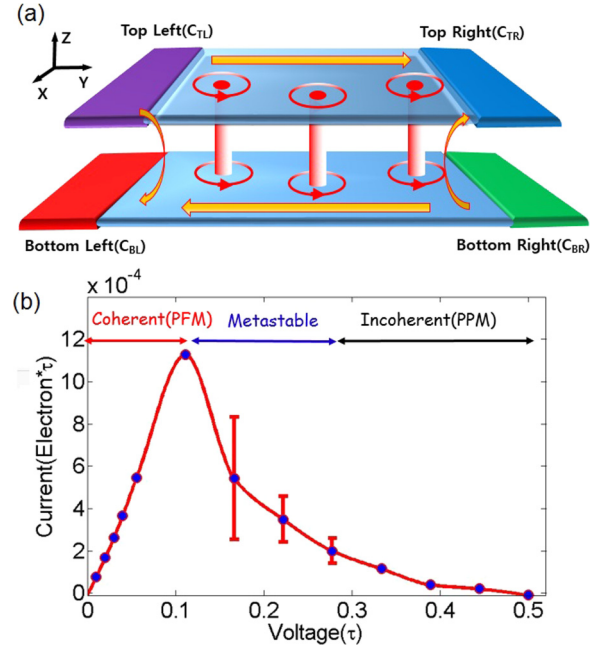

FIG. 1. (a) Schematic illustration of a pseudospin ferromagnet with contacts attached to each of the edges of the system. The arrows indicate the directions of the inter- and interlayer quasiparticle motion in each layer. Above I_c the system proliferates charged vortices which propagate in the same direction within each layer. (b) Plot of the calculated time-averaged coherent tunneling current from C_{TL} to C_{BL} (C_{BR} to C_{TR}) as a function of interlayer bias. We obtain the experimentally expected behavior which may be associated with the existence of three distinct pseudospin regimes: coherent (PFM), metastable (PFM-PPM), and incoherent (PPM). The bars on the plot illustrate the range in time-averaged currents calculated via our model.

where lattice points i and j are the coordinates of the x and y directions. In Eq. (1), τ is the nearest-neighbor hopping energy, which we have set to be $\tau = 2\tau_{\mathrm{trans}} = \pm 1$ (with the plus for the top layer and the minus for the bottom) for the calculations presented in this work. We choose the value of $|\tau_{\mathrm{trans}}| = 0.5$ so that the range of the voltage we apply during the simulation does not exceed the top or the bottom of the transverse-mode band. This choice allows the current flow through the device to exceed the critical current of the condensate. We may now generalize our single-layer Hamiltonian to the double-layer Hamiltonian by coupling the top and bottom layers [18,32],

$$\mathcal{H}_{\mathrm{sys}} = \begin{bmatrix} H_T & 0 \\ 0 & H_B \end{bmatrix} + \sum_{i=x,y} \Delta_i \otimes \sigma_i, \quad (2)$$

where σ_i represents the Pauli spin matrices acting on the layer degrees of freedom and $\otimes$ represents the Kronecker product. In Eq. (2), the first term on the right-hand side is the noninteracting contribution to the total Hamiltonian consisting of the single-layer Hamiltonians. The second term on the right-hand side represents the mean-field interlayer interaction term that consists of both single-particle tunneling and the mean-field many-body contribution resulting from the Coulomb interactions between the layers. Δ represents an effective pseudospin magnetic field and originates from the

interactions, will be explained later more fully in this section. As we are interested in the interacting physics between the two layers in a qualitative sense, we use a local-density approximation in which the interaction contribution between the layers is the on-site in-plane direction [18,32,33]. Additionally, full quantum many-body calculations have shown that the interlayer interaction is screened in the coupled-layer system, and thus, the local-density approximation we utilize in this work is reasonable [34]. As a result, each component of Δ in Eq. (2) is described using a typical mean-field decomposition as

$$
\begin{aligned}
\Delta_x &= \Delta_{\text{sas}} + U\langle m_{ps}^x\rangle, \\
\Delta_y &= U\langle m_{ps}^y\rangle,
\end{aligned}
\tag{3}
$$

where Δ_{sas} is the single-particle tunneling amplitude between the top and bottom layers. In Eq. (3), the terms $\langle m_{ps}^x\rangle$ and $\langle m_{ps}^y\rangle$ represent $\hat{x}$ and $\hat{y}$ directional pseudospin magnetizations that are a part of the overall pseudospin magnetization vector $\mathbf{m}_{ps}$, which we define as [20,31,33]

$$
\boldsymbol{m}_{ps} = \tfrac{1}{2}\,\text{Tr}[\rho_{ps}\sigma].
\tag{4}
$$

In Eq. (4), $\sigma = (\sigma_x,\sigma_y,\sigma_z)$ is a vector of the Pauli spin matrices, and ρ_{ps} is the 2×2 Hermitian pseudospin density matrix, which we define as

$$
\rho_{ps} = \begin{bmatrix} \rho_{\uparrow\uparrow} & \rho_{\uparrow\downarrow} \\ \rho_{\downarrow\uparrow} & \rho_{\downarrow\downarrow} \end{bmatrix}.
\tag{5}
$$

The interlayer exchange interactions defined in Eq. (3), $\langle m_{ps}^x\rangle$ and $\langle m_{ps}^y\rangle$, are obtained from the pseudospin density matrix as

$$
\begin{aligned}
\langle m_{ps}^x\rangle &= \tfrac{1}{2}(\rho_{\uparrow\downarrow} + \rho_{\downarrow\uparrow}), \\
\langle m_{ps}^y\rangle &= \tfrac{1}{2}(-i\rho_{\uparrow\downarrow} + i\rho_{\downarrow\uparrow}), \\
\langle m_{ps}^z\rangle &= \tfrac{1}{2}(\rho_{\uparrow\uparrow} - \rho_{\downarrow\downarrow}),
\end{aligned}
\tag{6}
$$

where $\rho_{\uparrow\downarrow}$ and $\rho_{\downarrow\uparrow}$ are the off-diagonal contributions to the pseudospin density matrix that arise due to the interactions between the two layers. In Eq. (6), we justify the omission of the exchange potential in the $\hat{z}$ direction because this contribution is small compared to the electrostatic potential difference between layers induced by the interlayer bias voltage quench. As a result, we may express the system Hamiltonian in terms of pseudospin field contributions,

$$
\mathcal{H}_{\text{sys}} = \begin{bmatrix} H_T & \Delta_x - i\Delta_y \\ \Delta_x + i\Delta_y & H_B \end{bmatrix}.
\tag{7}
$$

The planar pseudospin angle that will play a central role in the discussion below is defined as

$$
\phi_{ps} = \tan^{-1}\left[\frac{\langle m_{ps}^y\rangle}{\langle m_{ps}^x\rangle}\right].
\tag{8}
$$

This angle corresponds physically to the phase difference between electrons in the two layers.

With the system Hamiltonian defined, we select the parameters for the simulations, although the qualitative physics we address in this paper is irrespective of the parameter choices. In Eq. (3), we have set $U = -0.8$ and $\Delta_{\text{sas}} = 10^{-4}$. The initial populations of electrons and holes are set to result in half-filled

energy bands. Within each layer, we have 30×10 lattice points along the transport ($\hat{y}$) and transverse ($\hat{x}$) directions. For the transverse direction, we assumed periodic boundary conditions. Therefore, the order parameter is constant over the transverse direction. With the methodology established, we begin our calculations by obtaining the equilibrium density matrix ρ_{ps} self-consistently by iterating over the Hamiltonian, via Eq. (2). Our particular choice of parameters results in a condensate gap size of $\Delta_{DEC} = 0.009$.

B. Time evolution of pseudospin density matrix

After having self-consistently obtained the equilibrium pseudospin density matrix, we now seek the evolution of the system with time after a voltage quench has been applied. In order to incorporate the time-dependent dynamics associated with voltage quenches of the PFM, we must solve the TDKB equations [29,35] using as an input the self-consistently obtained equilibrium pseudospin density matrix at $t = 0$ as the starting point for the time evolution. The Kadanoff-Baym equation governs time propagation of the nonequilibrium pseudospin density matrix as

$$
(i\partial_t - \mathcal{H}_{\text{sys}})G_{\text{sys}}(t,t') = \delta(t,t') + \int dt_1 \Sigma(t,t_1)G_{\text{sys}}(t_1,t').
\tag{9}
$$

In Eq. (9), G_{sys} is the Green's function that connects nearest-neighbor points i and j as $G_{\text{sys}}^<(t) = i\langle c_j^\dagger c_i\rangle = i\rho_{ps}(t)$ [36], with ρ being the single-particle density matrix and $\Sigma(t,t')$ being the self-energy term. We may significantly reduce the complexity of the time propagation when the interactions are local in time. In this case, the off-diagonal time terms in the self-energy must vanish, resulting in a very simple expression for the self-energy, $\Sigma_{ij}(t,t') = \delta(t-t')v_{ji}G_{\text{sys}}^<(t,t')$, which includes the exchange interaction v_{ij}. Within the mean-field approximation, the interaction terms are always local in time, which justifies our methods. In order to obtain the time evolution of the density matrix, we solve Eq. (9) using a standard fourth-order Runge-Kutta method. Utilizing this result, we are capable of calculating the time evolution of the density matrix $\rho_{ps}(t)$ at any time $t > 0$ after the voltage is applied.

C. Review of pseudospin transfer torques

In this section, we briefly review the concept of pseudospin transfer torques [18,32,33,37–39], which will serve in interpreting the subsequent numerical results of the next section. In the DEC we consider here, the transport properties depend only on the quasiparticle Hamiltonian and on the chemical potentials within the leads. As we represent the $\hat{z}$ direction of the pseudospin orientation as the difference of the occupation numbers between the top layer and the bottom layer, the change in m_{ps}^z over time is given as a sum of intra- and interlayer currents. From the current conservation, the system must satisfy [39]

$$
\partial_t m_{ps}^z = -\boldsymbol{\nabla}\cdot\mathbf{j}^z - \frac{2}{\hbar}(\mathbf{m}_{ps}\times\Delta)_z,
\tag{10}
$$

where $\mathbf{j}^z$ is the $\hat{z}$ component of the pseudospin current contribution within the same layer. In Eq. (10), the contribution of $\mathbf{j}^z$ originates from the quasiparticles injected via the various layer contacts. The interlayer current contribution in the second term is rewritten as a cross product of the pseudospin density matrix $\mathbf{m}_{ps}$ and the interaction Δ. Note that the above representation of the current equation shows that the dynamics of the DEC behaves as a ferromagnet under the influence of an effective field Δ and injected pseudospin polarized current $\mathbf{j}^z$. In order to achieve steady-state transport, whereby Eq. (10) must go to zero, the injected current from the contact twists the angle between the pseudospin orientation and the exchange field to satisfy

$$2|\mathbf{m}_{ps}||\Delta|\sin(\phi_{ps} - \phi_\Delta) = 2\Delta_{\mathrm{sas}}m_{ps}^y = \hbar\nabla \cdot \mathbf{j}^z. \quad (11)$$

In Eq. (11), we define ϕ_Δ as the orientation of Δ within the $\hat{x}$-$\hat{y}$ plane. The pseudospin orientation does not align with the effective pseudospin exchange field that the injected quasiparticles experience because their pseudospin orientations must precess away from the injected pseudospin orientation as they move between layers in the bilayer system. The realignment of transport orbital pseudospin orientations in turn alters the total pseudospin and therefore the interaction contribution to Δ. As a result, the change in $\mathbf{m}_{ps} \times \Delta$ due to transport currents is referred to as the pseudospin transfer torque, in analogy with the terminology commonly found in metal spintronics. If the interlayer bias voltage drives a current, $\nabla \cdot \mathbf{j}^z$, that exceeds $I_c = 2\Delta_{\mathrm{sas}}\langle m_{ps}^y\rangle/\hbar$, or the maximal interlayer current that occurs when $\sin(\phi_{ps} - \phi_\Delta) = 1$, it will no longer be possible to achieve steady state as the condensate can no longer adjust its phase across the layer in order to accommodate current flow. Under these circumstances, the interlayer current will oscillate in sign, and the time-averaged current will be strongly reduced. In the next section, we show that DEC actually has an interesting nonequilibrium phase oscillating between the coherent and incoherent phases.

III. NUMERICAL RESULTS OF TIME-DEPENDENT NONEQUILIBRIUM DYNAMICS

With an understanding of the physics we expect, we now apply positive voltage to the top left contact ($V_{TL} = V_{\mathrm{int}}$) that serves to drive both interlayer and intralayer current flow within the dipolar exciton condensate for times $t > 0$. We examine the current flow into and out of each respective contact to determine the nonequilibrium dynamics and resultant phase diagram of the dipolar exciton condensate after a voltage quench. As we are interested in voltage-based phase transitions, we may delineate these phases with the definition of the critical voltage V_c or the interlayer voltage that results in the critical current I_c, thereby signaling the end of the PFM region. In Fig. 1(b), we plot the time-averaged interlayer coherence as a function of the bias applied to V_{TL}.

We immediately notice that Fig. 1(b) can be directly compared with the known experimental interlayer transport properties over the entire range of interlayer voltages [8]. Specifically, we recover the observed experimental trends in steady-state interlayer conductivity in PFM systems for $V_{TL} - V_c < 0$ and $\phi_{ps} \neq 0$, corresponding to the growth of the coherent tunnel current of the exciton condensate

with the applied voltage. In this case, when the system is in the PFM phase, the associated interlayer current [32,40] is

$$J_{\mathrm{int}}(r) = i[H, N_{\mathrm{top}}] = \Delta_{\mathrm{sas}}c_T^\dagger c_B - \Delta_{\mathrm{sas}}c_B^\dagger c_T = 2\Delta_{\mathrm{sas}}m_{ps}^y, \quad (12)$$

where $c_{T(B)}$ is a quasiparticle annihilation operator in the top (bottom) layer. In the PFM regime, when current is injected from C_{TL} (C_{TR}), an equal and opposite amount of current will flow into C_{BL} (C_{BR}). This perfect Coulomb drag may be understood from a simple analogy to Andreev reflections in superconductivity [18,26,32]. Within the PFM regime of a condensate, it is always possible to obtain a self-consistent steady-state solution between the equations of motion, the electrostatics, and the interactions with respect to global time-dependent phase rotation. In other words, the static limit of the Landau-Lifshitz-Slonczewski (LLS) equation must possess a solution [40].

When the applied voltage is equivalent to the critical voltage, $V_{TL} - V_c \approx 0$, the interlayer current reaches I_c, and we observe an abrupt drop in the magnitude of the interlayer current transfer in Fig. 1 along with a suppression of the interlayer Coulomb drag. This drop signals the termination of the purely PFM regime and the onset of an intermediate metastable regime. While the drop in interlayer charge transfer is expected based on the misalignment of the layer Fermi surfaces, the bars on the plot within Fig. 1(b) detailing the tunneling current indicate the presence of significant oscillations in the magnitude of the terminal currents within the metastable regime. This behavior is associated with the persistent launching of OPDs in both layers, which slows down the condensate velocity and recovers the coherent phase. Further increase in the applied potential, in which $V_{TL} - V_c \gtrsim \Delta$, shows that the magnitude of the interlayer current continues to decrease as the two layers become increasingly energetically separated. In this range of voltages, the system is in the incoherent, or PPM, phase, in which the magnitude of the interlayer current is governed solely by the value of Δ_{sas}, in agreement with previous experimental results [8,9].

To form a more complete understanding of the nature of the terminal currents past V_c, we examine the resulting terminal currents and $|m_{ps}|$ for several interlayer voltages, each resulting in $V_{TL} > V_c$. In Fig. 2(a), we apply a bias of $V_{TL} = 0.184$ that results in a current within the metastable regime. Indeed, in Fig. 2(a), we see that each of the terminal currents begins to stably oscillate, with the largest-magnitude oscillations appearing in I_{TR} and I_{BR}. These oscillations are signatures of competition between the PFM and PPM phases with a frequency consistent with the ac Josephson frequency proportional to $e(V - V_c)/h$ [41,42] (see the Supplemental Material [43] for numerical confirmation of the frequency dependence). Its maximum value is limited by the excitonic gap size, which corresponds to a frequency of 16.7 GHz, using the experimentally measured value of the gap [44]. The coherence between the layers triggers an electron current in the top layer and an equivalent hole current flow in the bottom layer. Time-averaged current flow in the bottom layer is lower than in the top layer as a consequence of the partial
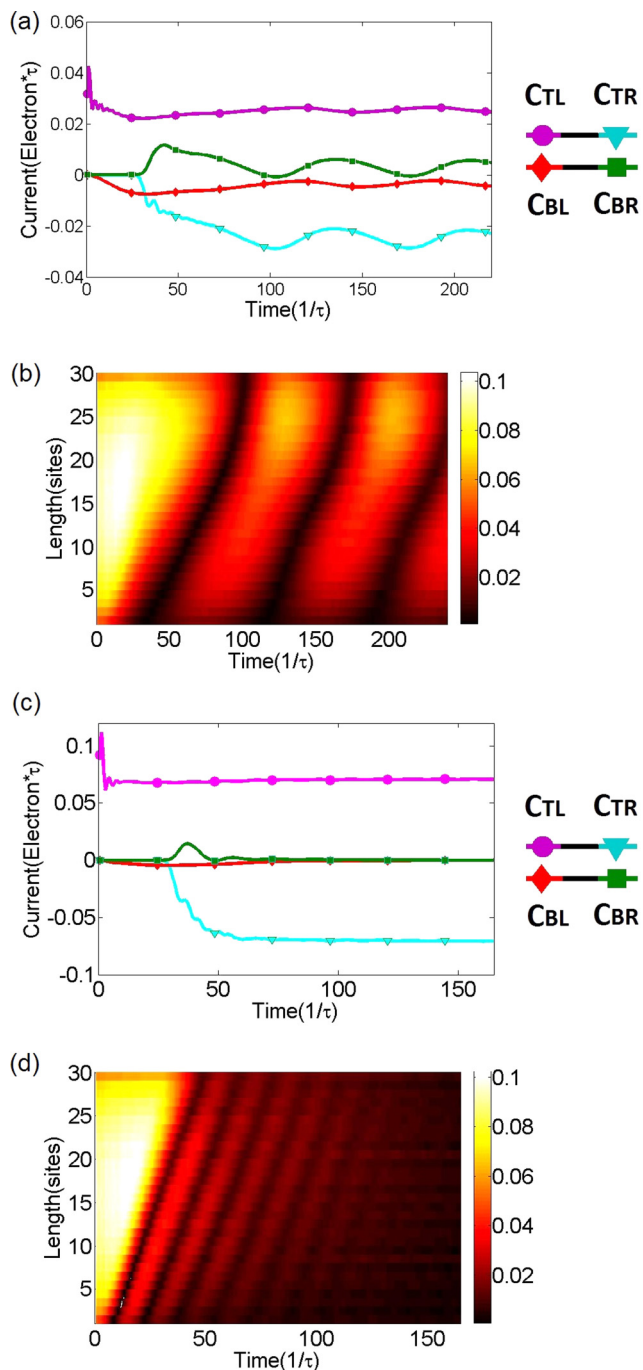
FIG. 2. Time evolution of the order parameter and the terminal current for (a) and (b) the metastable regime and (c) and (d) the PPM regime. (a) Plot of the terminal currents versus time for $V_{TL} = 0.184$ for the layers containing 30×10 points in the computational space. (b) Plot of the magnitude of the pseudospin order parameter as a function of time and length. (c) Plot of the terminal currents versus time for $V_{TL} = 0.5$. (d) Plot of the magnitude of the pseudospin order parameter as a function of time and length.

suppression of coherence brought about by the competition between the two distinct phases and nonzero spatial overlap between successive OPDs. At minimum points of I_{BR} and I_{TR}, the layers temporarily lose coherence. The loss of coherence results in I_{BR} possessing nearly zero value and a peak in I_{TR}

indicating that the observed behavior is associated with the negative density fluctuations.

Beyond V_c, we expect there is nonzero electric field inside the system, which accelerates the exciton pairs across the system and is approximately given by $E \approx (V_{TL} - V_c)/L$. By launching the defect, the phase gradient is reduced, and the exciton pairs in the PFM phase are decelerated in order to keep a constant superfluid velocity. To be more specific, when ϕ_{ps} winds into the $\hat{z}$ direction, the system launches an electronlike OPD that flows from the left of the system to the right at an applied bias of $V_{TL} = 0.184$, as seen in Fig. 2(b). The OPDs are topological defects [45,46] that break the order of the condensate and retain pseudospin order that points solely in the $\hat{z}$ direction. The corresponding zeros in $|m_{ps}|$ are accompanied by a π phase slip in the condensate, after which coherence is restored within the DEC. Therefore, the stable oscillations in the terminal currents are attributed to voltage-driven fluctuations between the PFM and PPM phases characterized by the entering and exiting of the OPD pair from the contacts. The maxima in I_{BR} and I_{TR} indicate that the coherence is recovered after the fluctuation passes. In Fig. 2(a), the condensate is not fully recovered at maximum points as the OPD bound states are not fully localized and the nonzero spatial overlap between bound states forms the discrepancy with the strong interaction limit.

In Fig. 2(c), we see another transition from the intermediate metastable oscillations between PFM and PPM phases to a stable PPM phase, which arises when m_z dominates the pseudospin orientation. In this regime, the bias-induced energy separation between the two layers wins a competition with the coherence of the bilayer. As a result, in the PPM phase, the current flows from C_{TL} to C_{TR} with only a transient response in C_{BL} and C_{BR}. Yet within the transient regime the current flowing to the lead C_{BR} is positive, indicating the presence of transient interlayer coherence in the system. Figure 2(d) shows the exponential decay of order parameter magnitude as the exchange enhancement is lost and the value asymptotes towards the noninteracting Δ_{sas} with ϕ_{ps} pointing in the $\hat{z}$ direction. It is critical to note that, in a closed system, the transition to the PPM phase is forbidden since total magnetic moment in the $\hat{z}$ direction $m_{z-tot} = \sum_i m_z$ is a roughly conserved quantity within the time scale $1/\Delta_{sas}$. However, open contacts act as a thermal reservoir that exchanges both energy and pseudospin. Thus, the existence of the reservoir allows the thermalization to the PPM state. In other words, at $t > 0$, direct insertion and extraction of pseudospin (quasiparticles) through open contact can relax the system to the PPM phase.

To more clearly illustrate voltage-induced phase transition, Fig. 3 shows the trajectory of normalized pseudospin evolution along the Bloch sphere. Figure 3(a) shows the oscillatory behavior between the PFM and PPM phases characteristic of the metastable phase as the pesudospin orientation precesses in the x-y plane. It precesses out of the plane to touch the z axis before returning to the x-y plane when a launched OPD passes through the observation point. Afterwards, the orientation returns to the x-y plane, and we observe persistent precession in its orbit until the next OPD reaches the observation point. The pseudospin precession within the x-y plane is a consequence of global phase evolution and the acceleration of
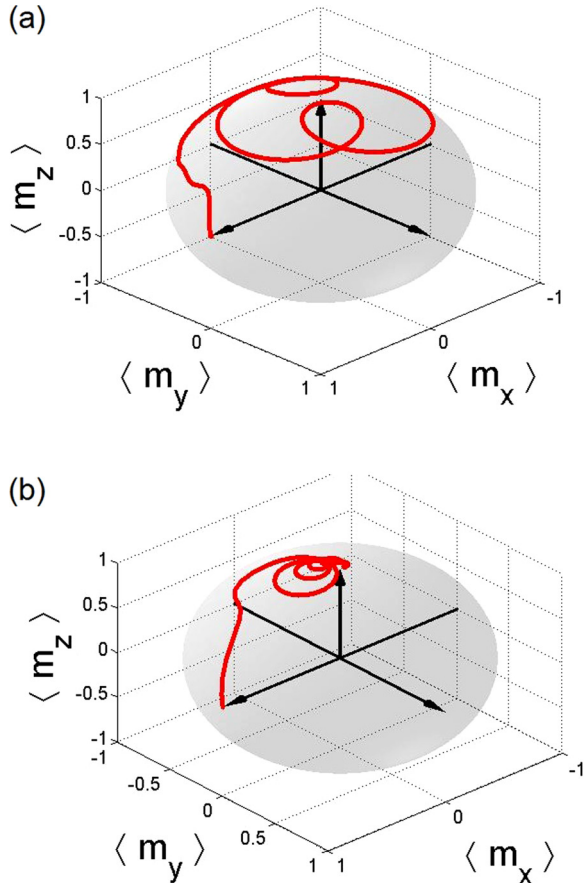
(a)

(b)

FIG. 3. Time evolution of pseudospin orientation at $x = 5$ lattice points for (a) the intermediate PFM-PPM metastable oscillations at an applied bias of $V_{TL} = 0.184$ and (b) the PPM phase at an applied bias of $V_{TL} = 0.5$. Each of these plots is taken within the time frame of a couple of phase-slip periods for visual simplicity.
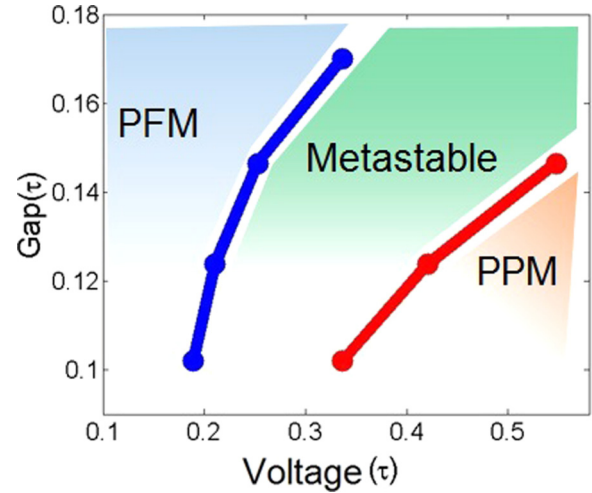

FIG. 4. Phase boundaries of PFM-metastable transition (blue circles) and metastable-PPM transition (red circles). The phases are calculated within a given time window of 10 fs. For each point on the blue curve, we use interaction strengths of $U = -0.85, 0.9, 0.95, 1$, while for the red curve, $U = -0.85, 0.9, 0.95$ are used.

the superfluid. When the pseudospin phase touches the north pole of the pseudospin Bloch sphere, it winds once about the pole as a direct reflection of the presence of the OPD. The regression of the pseudospin to the x-y plane indicates the recovery of phase coherence. In Fig. 3(b), the excessive bias breaks the coherence between the layers, forcing the transition from the PFM phase to the PPM phase. After the initial transient behavior, the pseudospin phase angle eventually precesses into the z direction, consistent with the current-induced phase transition to the PPM phase. In the transient regime before the PPM phase is fully established, pseudospin winds around the north pole several times before reaching its stable out-of-plane orientation along the pseudospin Bloch sphere and confirming the quenched phase transition.

Based on our results, it is clear that there is a dependence of the locations of the phase transitions on the strength of the interlayer interactions. We explore this relationship in Fig. 4, which shows the interaction strength dependence of the phases. We find that the location of the phase boundary of the PFM-PPM metastable transition, defined to be a point where two OPDs are launched within 10 fs, is proportional to the excitonic gap. In Fig. 4, we find a clear linear dependence of V_c on Δ when we examine the location of the phase transition between the PFM and PFM-PPM metastable phases. As the

gap size increases with the increase in the interaction strength, the PFM phase stability to changes in interlayer voltage increases in concert with the critical voltage V_c, which also moves to higher interlayer voltages. Additionally, we observe a similar trend in the transition between the metastable and PPM regions. In this work, we define the metastable-PPM transition to be the point at which the interlayer coherence decreases to 30% of the initial self-consistently obtained value. In the zero-gap limit, we know that both the PFM and the PFM-PPM metastable phase must vanish. Therefore, in the limit of the infinite-time response, the intersection of the two boundaries must meet at the origin of the plot. In Fig. 4, the intersection of the two lines is shifted from the origin due to the nature of time-dependent simulation. As we always have a finite time window within the simulation methodology associated with the TDKB formalism, it is inevitable that setting criteria to determine the location of a phase transition from a given finite-time simulation will result in discrepancies when compared to the infinite-time limit. These criteria give a time-scale cutoff which shifts the phase boundaries from the infinite-time response limit.

IV. SUMMARY AND CONCLUSIONS

In conclusion, we have studied the nonequilibrium time-dependent dynamics of dipolar exciton condensate phases focusing on the behavior past V_c via the time-dependent Kadanoff-Baym equations in coupled 2D layers. We have explained the salient features within the dipolar exciton condensate using the language of pseudospin ferromagnetism. We have demonstrated that, using this nonperturbative approach, we are able to completely reproduce the well-known experimental interlayer transfer characteristics associated with dipolar exciton condensates in quantum Hall semiconductor bilayers without assuming the phase of the system. We have shown that for voltages $V_{TL} - V_c < 0$, the system

exhibits pseudospin ferromagnetism denoted by perfect drag counterflow between the two layers. As the interlayer voltage is increased past the critical voltage, $V_{TL} - V_c \approx 0$, the system exhibits stable oscillation between the pseudospin ferromagnet phase and the pseudospin paramagnet phase. The voltage-induced oscillation between the two phases manifests as persistent oscillations in terminal currents corresponding to the continuous launching OPDs across the superfluid with a characteristic ac Josephson frequency. When the interlayer bias exceeds, $V_{TL} - V_c \gtrsim \Delta$, we have shown that the coherence between the layers is destroyed and the system transitions into the pseudospin paramagnet phase in which the interlayer transport is limited by single-particle tunneling.

[1] M. A. Baranov, M. S. Mar'enko, V. S. Rychkov, and G. V. Shlyapnikov, Phys. Rev. A **66**, 013606 (2002).

[2] Z. Hadzibabic, P. Krüger, M. Cheneau, B. Battelier, and J. Dalibard, Nature (London) **441**, 1118 (2006).

[3] T. W. Neely, E. C. Samson, A. S. Bradley, M. J. Davis, and B. P. Anderson, Phys. Rev. Lett. **104**, 160401 (2010).

[4] A. C. Potter, E. Berg, D. W. Wang, B. I. Halperin, and E. Demler, Phys. Rev. Lett. **105**, 220406 (2010).

[5] R. B. Balili, V. Hartwell, D. Snoke, L. Pfeiffer, and K. West, Science **316**, 1007 (2007).

[6] S. Christopoulos, G. Baldassarri, Hörger von Högersthal, A. Grundy, P. G. Lagoudakis, A. V. Kavokin, J. J. Baumberg, G. Christmann, R. Butté, E. Feltin, J. F. Carlin, and N. Grandjean, Phys. Rev. Lett. **98**, 126405 (2007).

[7] L. V. Butov, A. C. Gossard, and D. S. Chemla, Nature (London) **418**, 751 (2002).

[8] Y. Yoon, L. Tiemann, S. Schmult, W. Dietsche, K. von Klitzing, and W. Wegscheider, Phys. Rev. Lett. **104**, 116802 (2010).

[9] D. Nandi, T. Khaire, A. D. K. Finck, J. P. Eisenstein, L. N. Pfeiffer, and K. W. West, Phys. Rev. B **88**, 165308 (2013).

[10] M. Kellogg, J. P. Eisenstein, L. N. Pfeiffer, and K. W. West, Phys. Rev. Lett. **93**, 036801 (2004).

[11] E. Tutuc, M. Shayegan, and D. A. Huse, Phys. Rev. Lett. **93**, 036802 (2004).

[12] D. Snoke, S. Denev, Y. Liu, L. Pfeiffer, and K. West, Nature (London) **418**, 754 (2002).

[13] L. Tiemann, W. Dietsche, M. Hauser, and K. von Klitzing, New J. Phys. **10**, 045018 (2008).

[14] N. W. Sinclair, J. K. Wuenschell, Z. Vörös, B. Nelsen, D. W. Snoke, M. H. Szymanska, A. Chin, J. Keeling, L. N. Pfeiffer, and K. W. West, Phys. Rev. B **83**, 245304 (2011).

[15] B. Dellabetta and M. J. Gilbert, J. Comput. Electron. **12**, 248 (2013).

[16] H. Min, R. Bistritzer, J. J. Su, and A. H. MacDonald, Phys. Rev. B **78**, 121401 (2008).

[17] M. J. Gilbert and J. Shumway, J. Comput. Electron. **8**, 51 (2009).

[18] M. J. Gilbert, Phys. Rev. B **82**, 165408 (2010).

[19] B. Seradjeh, J. E. Moore, and M. Franz, Phys. Rev. Lett. **103**, 066402 (2009).

[20] Y. Kim, E. M. Hankiewicz, and M. J. Gilbert, Phys. Rev. B **86**, 184504 (2012).

[21] G. Y. Cho and J. E. Moore, Phys. Rev. B **84**, 165101 (2011).

[22] D. Tilahun, B. Lee, E. M. Hankiewicz, and A. H. MacDonald, Phys. Rev. Lett. **107**, 246401 (2011).

[23] J. C. Budich, B. Trauzettel, and P. Michetti, Phys. Rev. Lett. **112**, 146405 (2014).

[24] R. V. Gorbachev, A. K. Geim, M. I. Katsnelson, K. S. Novoselov, T. Tudorovskiy, I. V. Grigorieva, A. H. MacDonald, S. V. Morozov, K. Watanabe, T. Taniguchi, and L. A. Ponomarenko, Nat. Phys. **8**, 896 (2012).

[25] J. P. Eisenstein and A. H. MacDonald, Nature (London) **432**, 691 (2004).

[26] J. J. Su and A. H. MacDonald, Nat. Phys. **4**, 161 (2008).

[27] M. Heyl, A. Polkovnikov, and S. Kehrein, Phys. Rev. Lett. **110**, 135704 (2013).

[28] P. Myohanen, A. Stan, G. Stefanucci, and R. van Leeuwen, Phys. Rev. B **80**, 115107 (2009).

[29] G. Stefanucci and R. van Leeuwen, *Nonequilibrium Many-Body Theory of Quantum Systems* (Cambridge University Press, Cambridge, 2013).

[30] T. Hyart and B. Rosenow, Phys. Rev. Lett. **110**, 076806 (2013).

[31] A. H. MacDonald, Phys. B (Amsterdam, Neth.) **298**, 129 (2001).

[32] Y. Kim, A. H. MacDonald, and M. J. Gilbert, Phys. Rev. B **85**, 165424 (2012).

[33] E. Rossi, A. S. Nunez, and A. H. MacDonald, Phys. Rev. Lett. **95**, 266804 (2005).

[34] J. Shumway and M. J. Gilbert, Phys. Rev. B **85**, 033103 (2012).

[35] A. Stan, N. E. Dahlen, and R. V. Leeuwen, J. Chem. Phys. **130**, 224101 (2009).

[36] E. Perfetto, G. Stefanucci, and M. Cini, Phys. Rev. B **82**, 035446 (2010).

[37] L. Ozyuzer, Y. Simsek, H. Koseoglu, F. Turkoglu, C. Kurter, U. Welp, A. E. Koshelev, K. E. Gray, W. K. Kwok, T. Yamamoto, K. Kadowaki, Y. Koval, H. B. Wang, and P. Müller, Supercond. Sci. Technol. **22**, 114009 (2009).

[38] A. A. Burkov and A. H. MacDonald, Phys. Rev. B **66**, 115320 (2002).

[39] A. S. Nunez, R. A. Duine, P. Haney, and A. H. MacDonald, Phys. Rev. B **73**, 214426 (2006).

[40] J. J. Su and A. H. MacDonald, Phys. Rev. B **81**, 184523 (2010).

[41] H. A. Notarys and J. E. Mercereau, Physica **55**, 424 (1971).

[42] A. J. Leggett, Rev. Mod. Phys. **73**, 307 (2001).

[43] See Supplemental Material at http://link.aps.org/supplemental/10.1103/PhysRevB.94.214307 for the numerical confirmation of the Josephson frequency.

[44] P. Giudici, K. Muraki, N. Kumada, and T. Fujisawa, Phys. Rev. Lett. **104**, 056802 (2010).

[45] For a review, see S. M. Girvin and A. H. MacDonald, in *Perspectives in Quantum Hall Effects*, edited by A. Pinczuk and S. Das Sarma (Wiley, New York, 1997) pp. 161–224.

[46] K. Moon, H. Mori, K. Yang, S. M. Girvin, A. H. MacDonald, L. Zheng, D. Yoshioka, and S.-C. Zhang, Phys. Rev. B **51**, 5138 (1995).